

Effects of Compound Structure on Carbazole Dication–DNA Complexes: Tests of the Minor-Groove Complex Models

Farial A. Tanious, Daoyuan Ding, Donald A. Patrick,[‡] Christian Bailly,[§] Richard R. Tidwell,[‡] and W. David Wilson*

Department of Chemistry and Laboratory for Chemical and Biological Sciences, Georgia State University, Atlanta, GA, 30303, Department of Pathology, University of North Carolina, Chapel Hill, North Carolina 27599, INSERM U-524 et Laboratoire de Pharmacologie Antitumorale du Centre Oscar Lambret, IRCL, Place de Verdun, 59045 Lille, France

Received May 31, 2000; Revised Manuscript Received July 11, 2000

ABSTRACT: Carbazole dications have shown excellent activity against opportunistic infections, but they are quite different in structure from previously studied unfused aromatic cations that function by targeting the DNA minor groove. In a previous report [Tanious, F. A., Ding, D., Patrick, D. A., Tidwell, R. R., and Wilson, W. D. (1997) *Biochemistry* 36, 15315–15325] we showed that, despite their fused ring structure, the carbazoles also bind in A/T sequences of the DNA minor groove and we proposed models for the carbazole–DNA complexes with the carbazole nitrogen facing out of the groove for 3,6 substituted compounds but into the groove in 2,7 carbazoles. To test and refine the models, carbazole-*N*-methyl substituted derivatives have been synthesized in both the 3,6 and 2,7 series as well as a new 2,6 substituted NH derivative that is intermediate in structure. Footprinting results indicate a broad AT specificity of carbazole binding and a pattern in agreement with a minor groove complex. Surface plasmon resonance biosensor analysis of carbazole binding to an oligomer with an AATT central sequence indicated that the 2,7 NH compound has the largest binding constant. Both the 3,6 NH and NMe compounds bind with similar equilibrium constants that are less than for the 2,7 NH compound. The 2,7 NMe compound has the lowest binding constant of all the carbazoles. Spectroscopic results are also similar for the two 3,6 derivatives but are quite different for the 2,7 NH and NMe carbazole dications. Structural analysis of carbazole complexes with an AATT sequence by 2D NMR methods also supported a minor groove complex of the carbazoles in orientations in agreement with the previously proposed models. From these results, it is clear that the fused ring carbazoles can bind strongly in the DNA minor groove with a broad A/T specificity and that the 2,7 and 3,6 substituted carbazoles bind to the minor groove in opposite orientations.

The effect of opportunistic infections (OI)¹ on immune-compromised populations has been known for decades but the recent AIDS epidemic has sparked renewed interest in the development of new anti-OI agents (1–4). The mechanism of action of a series of dicationic unfused-aromatic compounds, which have excellent anti-OI activity, is believed to involve initial binding of the drug to AT sequences in the minor groove of DNA with subsequent selective inhibition of a DNA directed microbial enzyme (1–4). Most organic dications that bind in the minor groove of DNA have

extended conjugated systems with unfused aromatic rings that are directly bonded or connected through linking groups, and cationic amidine groups or amidine derivatives (5–15). These compounds can assume a shape that closely matches the DNA minor groove (10–12). Pentamidine, which is being used clinically against *Pneumocystis carinii pneumonia* (PCP), a leading cause of morbidity and mortality in AIDS patients (1–4), has the aromatic groups linked through an alkyl chain. Considerable evidence indicates that the mechanism of action of pentamidine and analogues involves formation of a complex with the DNA of the microorganism, followed by selective inhibition of a DNA-directed microbial enzyme (1–4). Pentamidine binds in the DNA minor groove in AT sequences (16, 17), but it shows some side effects that limit its use (2).

As part of our extended investigations to develop new anti-OI drugs with improved therapeutic properties and to characterize their interactions with DNA (14–20), we have investigated the binding of new 2,7 and 3,6 carbazole dications (structures in Table 1) to DNAs of different sequence (21, 22). The carbazole derivatives have quite different structures than the compounds discussed above but they exhibit some of the best anti-*Pneumocystis* activity

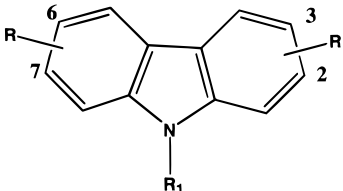
[†] This work was supported by NIH Grants to W.D.W. (GM-61587; AI-33363) and to R.R.T. (AI-33363) and from the Ligue Nationale Française Contre le Cancer to C.B. Instrumentation was purchased through funds from the Georgia Research Alliance.

* To whom correspondence should be addressed. Phone: (404) 651-3903. Fax: (404) 651-2751. E-mail: chewdw@panther.gsu.edu.

[‡] University of North Carolina.

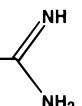
[§] INSERM U-524 et Laboratoire de Pharmacologie Antitumorale du Centre Oscar Lambret.

¹ Abbreviations: OI, opportunistic infections; PCP, *Pneumocystis carinii pneumonia*; SPR, surface plasmon resonance; RU, response units; Tm, thermal melting; NMR, nuclear magnetic resonance; NOESY, nuclear Overhauser enhancement spectroscopy; COSY, homo-nuclear correlated spectroscopy; CD, circular dichroism; MES, 2-(*N*-morpholino)ethanesulfonic acid; EDTA, ethylenediamine tetraacetic acid, DSS, 2,2-dimethyl-2-silapentane-5-sulfonate, sodium salt.

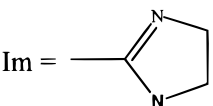
Table 1: Structures and T_m of the Carbazole Compounds with 1–337


compd	position of R	R	R1	ΔT _m /oligo
2,7CN–H	2,7	Am	H	10.9
3,6CN–H	3,6	Am	H	8.2
2,6CN–H	2,6	Am	H	6.5
3,6CN–Me	3,6	Am	CH ₃	7.5
3,6CN–H–Im	3,6	Im	H	7.8
2,7CN–H–Im	2,7	Im	H	12.0
2,7CN–Me	2,7	Im	CH ₃	6.3

Am =



Im =



in the dication series (21). The fused-ring carbazoles look more like classical intercalators than groove binding agents, but based on kinetic and spectroscopic, particularly NMR, results we have reported the surprising finding that both the 3,6 and 2,7 compounds bind in the minor groove in AT sequences despite their quite different and fused aromatic structures (22). They represent new models for minor-groove binding that are, however, closely related to the models obtained for unfused systems. A second initially surprising feature of the carbazole–DNA interactions is that the proposed interaction mode of the 3,6 carbazole has the carbazole NH group pointed out of the DNA minor groove while with the 2,7 derivative the NH points into the groove and is directly involved in carbazole–DNA complex formation (22). To test these proposed models and to define their generality and limits as well as probe the sequence-recognition specificity of the carbazoles in more detail, we have synthesized several new derivatives and investigated their DNA interactions. We have encountered a number of difficulties in spectroscopic analysis of the complexes, but we report here that binding can be quantitatively characterized with surface plasmon resonance biosensor technology. We have also determined the DNA binding sequence specificity of the different carbazoles with DNase I footprinting techniques.

Compound Design. The carbazole binding models predict that both amidine and imidazoline substituted compounds should bind quite well in the DNA minor groove in AT sequences, and both types of cations have been synthesized in the 3,6 and 2,7 NH carbazole series to test this point (Table 1). NMe derivatives were synthesized since replacing the carbazole NH with an NMe should have little effect on the 3,6 complex where the carbazole NH is predicted by our models to point out of the groove. With the 2,7 complex, however, the NH is predicted to point into the groove and an NMe substituent should disrupt many of the carbazole–DNA interactions and decrease affinity. A 2,6 derivative that is a combination of the 3,6 and 2,7 compounds was synthesized and is predicted to be able to form DNA contacts similar to those of the 2,7 carbazole with the NH of the

carbazole pointed into the groove. The 2,6 compound can form only half the hydrogen bonds to DNA as the 3,6 carbazole with the NH pointed out of the groove and such a complex should be energetically disfavored. The results reported here are divided into three sections that are designed to answer the following questions about the carbazole–DNA interaction: (i) what are the primary DNA recognition sequences for the compounds; (ii) what is the binding mode in these DNA sequences; and (iii) how strongly do the compounds bind to the sequences?

MATERIALS AND METHODS

Compounds, Biochemicals, and Buffers. The carbazole derivatives were prepared as reported previously (21) and the synthesis of the 2,6 derivative will be published elsewhere. Purity of all compounds was verified by NMR and elemental analysis.

Nucleoside triphosphates labeled with ³²P (α-dATP and γ-ATP) were obtained from Amersham. Unlabeled dATP, restriction endonucleases *Eco*RI, *Ava*I, and *Pvu*II were from Boehringer Mannheim (Germany). Alkaline phosphatase, T4 polynucleotide kinase, and avian myeloblastosis virus reverse transcriptase (Boehringer Mannheim) were used according to the supplier's recommended protocol in the activity buffer provided. Bovine pancreatic deoxyribonuclease I (DNase I, Sigma Chemical Co.) was stored as a 7200 units/mL solution in 20 mM NaCl, 2 mM MgCl₂, 2 mM MnCl₂, pH 8.0. The stock solutions of DNase I were kept at –20 °C and freshly diluted to the desired concentration immediately prior to use. All other chemicals were analytical grade reagents, and all solutions were prepared using doubly deionized, Millipore filtered water. MES buffers contained 0.01 M MES and 10^{–3} M EDTA with the pH adjusted to 6.2 with NaOH and sodium chloride added to adjust the ionic strength to the desired value. Phosphate buffer for NMR experiments contained 7.5 mM sodium phosphate, 100 mM NaCl, and 0.01 mM EDTA, pH 7.0.

DNA Polymers and Oligomers. Poly[d(A–T)]₂ (Pharmacia) was prepared as previously described (23). Three different AATT containing oligomers (Midland Certified Reagent Co.—HPLC purified and desalted) were used in these studies: the 5'-biotin labeled hairpins d(biotin-CGAATTCGCTCTCGAATTCG) (hairpin loop underlined) was used in surface plasmon resonance studies; the self-complementary 10mer d(GCGAATTCGC) was used for NMR; and the self-complementary 12mer d(CGCGAATTCGCG) was used for melting studies. The oligomer concentrations were determined optically using extinction coefficients per mole of strand at 260 nm determined by the nearest neighbor procedure (24).

Purification and Radiolabeling of the DNA Substrates for Footprinting. Plasmids pBS (Stratgene, La Jolla, CA) and pLAZ (25) and pKMp27 (26) were prepared from *E. coli* according to standard procedures employing sodium dodecyl sulfate-sodium hydroxide lysis followed by purification using Qiagen columns. The 117-mer fragment from plasmid pBS was rendered radioactive by 3'-[³²P]-end labeling of the *Eco*RI–*Pvu*II double digest of the plasmid using [α-³²P]-dATP (6000 Ci/mmol) and avian myeloblastosis virus reverse transcriptase. The 155-mer fragment was prepared by 5'-[³²P]-end labeling of the *Eco*RI/alkaline phosphatase treated plasmid using [γ-³²P]ATP (6000 Ci/mmol) and T4 poly-

nucleotide kinase followed by treatment with *Pvu*II. The labeled digestion products were separated on a 6% polyacrylamide gel under nondenaturing conditions in TBE buffer (89 mM Tris-borate pH 8.3, 1 mM EDTA). After autoradiography, the requisite gel band of DNA was excised, crushed, and soaked in elution buffer (500 mM ammonium acetate, 10 mM magnesium acetate) overnight at 37 °C. This suspension was filtered through a Millipore 0.22 μ m filter and the DNA was precipitated with ethanol. Following washing with 70% ethanol and vacuum-drying of the precipitate, the labeled DNA was resuspended in 10 mM Tris adjusted to pH 7.0 containing 10 mM NaCl.

Footprinting Experiments. Cleavage reactions by DNase I were performed essentially according to the protocol previously described (27). Reactions were conducted in a total volume of 10 μ L. Samples (3 μ L) of the labeled DNA fragment were incubated with 5 μ L of the buffer solution supplemented with the drug under test. After 30 min of incubation at 37 °C to ensure equilibration of the binding reaction, digestion was initiated by the addition of 2 μ L of the endonuclease solution whose concentration had been adjusted to limit the enzyme attack to less than 30% of the starting material so as to minimize the incidence of multiple cuts in any strand ("single-hit" kinetic conditions). Optimal enzyme dilutions were established in preliminary calibration experiments. Typically, DNase I experiments included 0.01 unit/mL enzyme, 20 mM NaCl, 2 mM MgCl₂, and 2 mM MnCl₂, pH 7.3. At the end of the reaction time (routinely 4 min at room temperature), the digestion was stopped by freeze-drying. After lyophilization, each sample was washed once with deionized water then lyophilized again prior to resuspending in 3 μ L of an 80% formamide solution containing tracking dyes (purchased from Sigma). DNA cleavage products were resolved by polyacrylamide gel electrophoresis under denaturing conditions (0.3 mm thick, 8% acrylamide containing 8 M urea). Electrophoresis was continued until the bromophenol blue marker had run out of the gel (about 2.5 h at 60 W, 1600 V in TBE buffer, BRL sequencer model S2). Gels were soaked in 10% acetic acid for 15 min, transferred to Whatman 3MM paper, dried under vacuum at 80 °C, and subjected to the phosphorimager. A Molecular Dynamics 425E PhosphorImager was used to collect data from storage screens exposed to the dried gels overnight at room temperature. Baseline-corrected scans were analyzed by integrating all the densities between two selected boundaries using ImageQuant version 3.3 software. Each resolved band was assigned to a particular bond within the DNA fragment by comparison of its position relative to sequencing standards generated by treatment of the DNA with dimethylsulfate (G) followed by piperidine-induced cleavage at the modified guanine bases.

Absorption, Fluorescence, and Circular Dichroism Spectroscopy. UV–vis scans were obtained in the presence and absence of DNA as previously described (28, 29) with a Cary 4 spectrophotometer in MES buffer with 0.1 M NaCl added. Fluorescence spectra in MES buffer were obtained in the presence and absence of DNA on a Photon Technology International (PTI) spectrometer with software that controls the instrument and collects the fluorescence data. CD spectra were obtained on a computer-controlled Jasco J-710 spectrometer with the software supplied by Jasco for instrument control and data acquisition. Solutions of the free compounds

and complexed with DNA in MES buffer at 25 °C were scanned in 1 cm quartz cuvettes.

DNA Thermal Melting. Thermal melting experiments were conducted with Cary 3 or Cary 4 spectrophotometers interfaced to microcomputers as previously described (30). A thermistor fixed into a reference cuvette was used to monitor the temperature. The DNA or oligomer was added to 1 mL of buffer (MES with 0.1 M NaCl added) in 1 cm path length reduced volume quartz cells, and the concentration determined by measuring the absorbance at 260 nm. Experiments were generally conducted at a concentration of 3×10^{-6} M in duplex for d(CGCGAATTCGCG)₂. For the complex Tm experiments a ratio of 1 compound per oligomer duplex for d(CGCGAATTCGCG)₂ was used.

Determination of Binding Constants by Surface Plasmon Resonance. Surface plasmon resonance (SPR) measurements were performed with a four-channel BIAcore 2000 system and streptavidin coated sensor chips (SA). To prepare the sensor chips for use, they were conditioned with three consecutive 1 min injections of 1 M NaCl in 50 mM NaOH followed by extensive washing with buffer. 5'-Biotinylated DNA (25 nM) in MES buffer with 0.1M NaCl was immobilized on the surface by noncovalent capture. Three flow cells were used to immobilize DNA samples and the fourth flow cell was left blank as a control. Manual injection was used with a flow rate of 2 μ L/min to achieve long contact times with the surface and to control the amount of the DNA bound to the surface. Samples of the drug were prepared in filtered and degassed buffer by serial dilutions from stock solutions. All procedures for binding studies were automated as methods using repetitive cycles of sample injection and regeneration. All the drug samples were injected from 7 mm plastic vials with pierceable plastic crimp caps at a flow rate of 20 μ L/min using the KINJECT command. For the carbazole–DNA complexes, buffer flow alone is sufficient to dissociate the carbazoles from DNA for surface regeneration. An array of different carbazole concentrations was used in each experiment and the results were analyzed as described below.

NMR. NMR spectra were obtained on a Varian Unity plus 600 spectrometer as previously described (14, 31). Data were processed either by Vnmr 5.1 software from Varian or with the program FELIX (Biosym Technologies, San Diego, CA). Typical conditions for the collection of spectra in D₂O included 6000 Hz spectral width, 2000 scans, 1-s relaxation delay, 0.6 mL sample in a 5 mm NMR tube, and 1.5 Hz line broadening before Fourier transformation. A relatively low concentration of drug (0.2 mM) was necessary both to prevent precipitation of the complexes and to ensure that no concentration induced shifts of the free drug were observed. Titrations were conducted over a range of drug–DNA ratios from 0.2 to 2.5 under fast exchange conditions (temperature ≥ 35 °C). Temperature studies were conducted from 25 to 85 °C. Spectral lines were very broad below 20 °C. All NMR spectra were obtained in phosphate buffer solution (7.5 mM NaH₂PO₄, 10^{-5} M EDTA, pH 7.0, 0.10 M NaCl). Samples were referenced to DSS (2,2-dimethyl-2-silapentane-5-sulfonate, sodium salt) using the calibrated position of the water peak relative to DSS. Assignment of the aromatic proton signals for the drug–DNA complexes were made via drug–DNA titrations, temperature effects in 1D, and 2D COSY experiments.

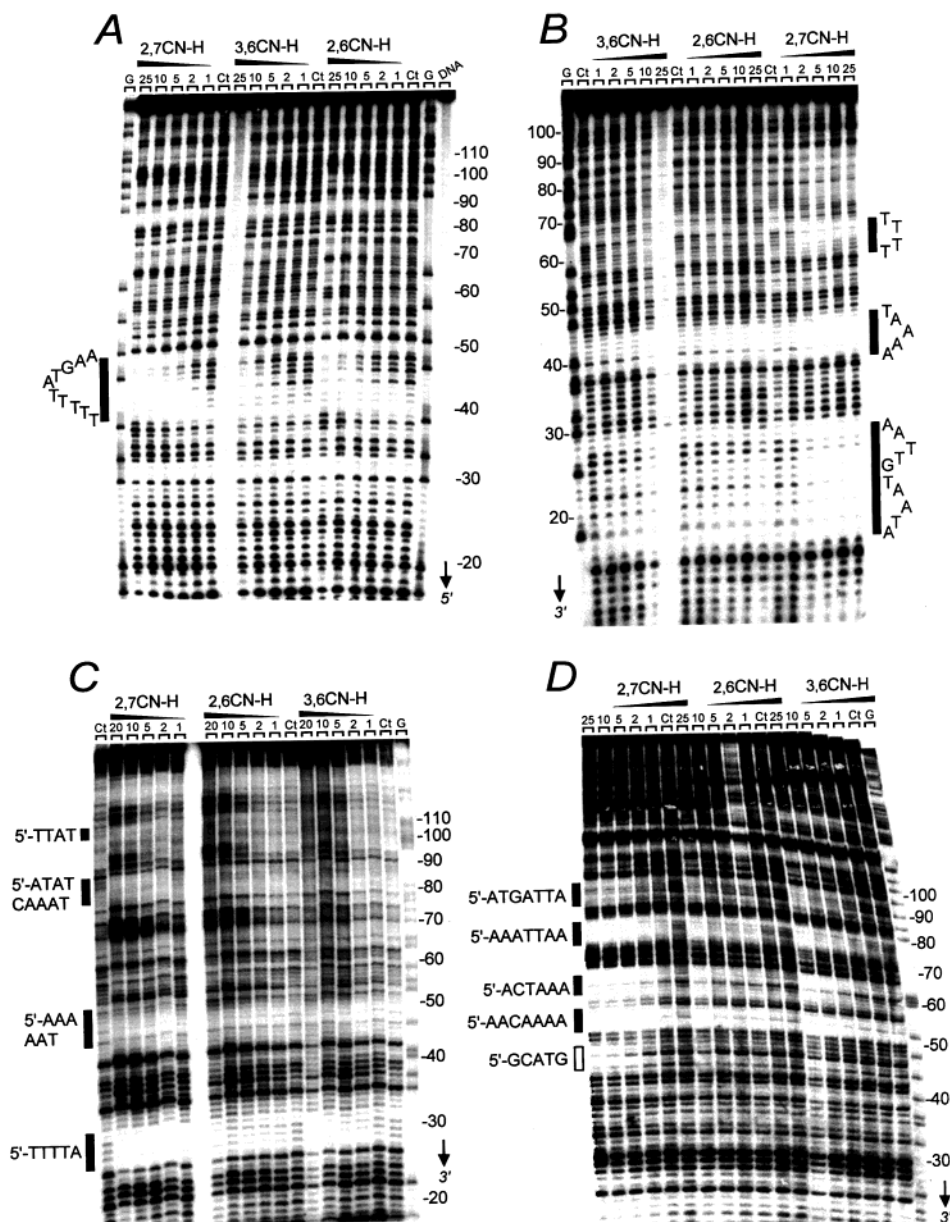


FIGURE 1: DNase I footprinting of the carbazoles on the (A) 155 bp, (B) 117 bp, (C) 160 bp and (D) 265 bp restriction fragments. In each case, the products of the DNase I digestion were resolved on an 8% polyacrylamide gel containing 8 M urea. Drug concentrations (μM) are indicated at the top of each lane. Tracks labeled control (Ct) contained no drug and tracks labeled G represent dimethylsulfate-piperidine markers specific for guanines. Numbers at the side of the gels refer to the numbering scheme of the fragments. The sequences and positions of the drug binding sites are indicated.

For the 1:1 ratio of DNA duplex to ligand, 1 mmol of the carbazole was added to 1 mmol of the DNA duplex solution in the NMR tube. The solvent was removed under N_2 , and 0.6 mL of 99.99% D_2O added and solvent removed several times. The sample was finally dissolved with 0.6 mL of 99.996% D_2O . All of the 1D and 2D ^1H spectra were collected on Varian Unity plus 500 or 600 MHz spectrometers and the data transferred to a Silicon Graphics workstation for processing with FELIX. One-dimensional experiments were obtained with a spectral width of 4500 Hz, 16 000 complex data points, a 1 s relaxation delay, 100–500 transients. Two-dimensional experiments were obtained with a spectral width of 6000 Hz in both dimensions with 1024 complex data points in the t_2 dimension and 512 points in the t_1 dimension. Phase sensitive NOESY spectra were

obtained with a mixing time of 300 ms using the method of States (32).

RESULTS

(I) *What Are the Primary DNA Recognition Sequences for the Compounds? DNase I Footprinting.* DNase I digestion patterns observed in the absence and presence of the three NH carbazole derivatives with a 155 bp fragment are illustrated in Figure 1A. The presence of 2 μM 2,7CN-H clearly alters the digestion pattern compared to that seen in the control lanes with DNA alone. Experiments conducted with the 2,6CN-H and 3,6CN-H derivatives gave comparable patterns of DNase I cutting, but a higher drug concentration (5–10 μM) is needed to observe a similar extent of footprinting. However, the strongly protected sequence (positions

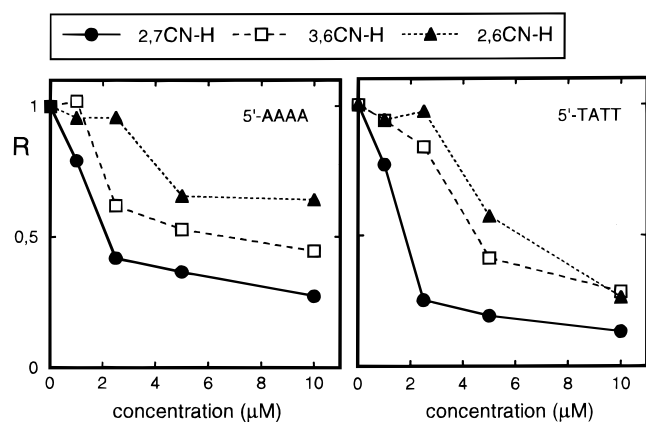


FIGURE 2: Footprinting plots for two selected AT sites in the 155-mer fragments. The relative band intensity R is plotted as a function of ligand concentration.

40 and 50) is the same for all three carbazoles: 5'-TTTT-TATGAA. With the 3,6CN-H derivative, concentrations greater than 20 μM gave no reliable information due to secondary binding and near-complete inhibition of the enzyme. The differences between primary and secondary binding are described in more detail below. To gain a more accurate impression of the drug specificity, intensities from selected gel lanes in Figure 1A were measured by densitometry and converted to numerical probabilities of cleavage. The footprinting plots in Figure 2 compare the binding of all three carbazole drugs to two AT sites within the 155 bp fragment: 5'-AAAA and 5'-TATT. In both cases, the cleavage protection was more pronounced with the 2,7CN-H compound compared to the 2,6CN-H and 3,6CN-H analogues. The drug concentrations required to reduce the cleavage by DNase I by 50% (C_{50} values) at the 5' TATT site are 0.8, 4, and 5 μM for 2,7CN-H, 3,6CN-H, and 2,6CN-H, respectively. At the 5'-AAA site, the drugs also rank in the order 2,7CN-H > 3,6CN-H > 2,6CN-H.

To extend the analysis of carbazole sequence specificity, similar DNase I footprinting experiments were performed using three other DNA fragments of 117, 160, and 265 bp (panels B, C, and D in Figure 1, respectively). The results are totally consistent with those obtained with the 155 bp DNA. In every cases, the 2,7CN-H compound produced more clear footprints than the 2,6 and 3,6 analogues. At some sites, such as 5'-TTTA on the 160 bp DNA (around positions 30 in Figure 1C) or 5'-TAAAA on the 117 bp DNA (around positions 45 in Figure 1B) the cutting by the enzyme is totally inhibited attesting that the site is fully blocked by the 2,7CN-H compound. At other sites blockages are weaker but always more pronounced with 2,7CN-H compared to 3,6CN-H and 2,6CN-H. Adjacent to the footprints (binding sites), regions of enhanced cleavage by DNase I often can be detected. These regions generally correspond to GC-rich sequences. For example, the 160 bp fragment offers the sequence 5'-CGCGCCGC (between positions 70 and 80) which is avidly cut by DNase I in the presence of 2,7CN-H. The presence of the drug greatly potentiates the cleavage by the enzyme at several GC-rich sequences, particularly in the 160 and 265 bp fragments. The 117 and 155 bp fragments do not offer long runs of GC sites. Although the mass-action effect described by Goodisman and Dabrowiak (33) can explain generally enhanced cleavage at unprotected sites, the

Table 2: Sequences in the DNA Fragments that Are Protected from Cleavage by DNase I in the Presence of 2,7CN-H Inferred from Differential Cleavage Plots^a

DNA	protected sequences
117-mer	
5'-AATTGTAATA	(20–29)
5'-TAAAA	(42–46)
5'-TTTT	(63–66)
155-mer	
5'-TTTTTATGAA	(39–48)
160-mer	
5'-TTTTA	(27–31)
5'-AAAAAT	(47–52)
5'-ATATCAAAT	(82–90)
5'-TTAT	(109–112)
265-mer	
5'-GCATG	(44–48)
5'-AACAAAA	(53–59)
5'-ACTAAA	(63–68)
5'-AAATTAA	(74–80)
5'-ATGATTA	(92–98)

^a The location of each sequence, with reference to the numbering schemes, is indicated in parentheses.

specific enhancement of cleavage at certain GC rich tracts would appear to be a consequence of conformational changes induced in the DNA by binding of the carbazole drugs to neighboring AT sites.

A total of 13 binding sites were identified within the four DNA fragments used in the footprinting experiments. With some fragments additional drug binding sites can be discerned at the top of the gels but they lie beyond the region accessible to densitometric analysis. The sequences protected from cleavage by 2,7CN-H are listed in Table 2. With one exception, all the binding sites contain at least four contiguous A•T bps. The exception is the sequence 5'-GCATG corresponding to positions 43–47 in the 265 bp fragment (site marked with an open rectangle for the panel D in Figure 1). We note that the DNase I cutting at this site is not reduced by 2,6CN-H and 3,6CN-H, and with 2,7CN-H it is inhibited to a much smaller degree than at (A/T)₄ sites. In some cases, the binding sites encompass just four contiguous A•T base pairs, but in other cases, the protected sequence can be longer. For example, a 9 bp site is observed between positions 82 and 90 on the 160-mer fragment (Table 2) in the sequence 5'-ATATCAAAT, and this suggests the juxtaposition of two sites, each being four base pairs in length.

To investigate further the sequence preference of the 2,7CN-H, we performed additional footprinting experiments with two fragments, named TAYB (131 bp) and TAYD (116 bp), which contain multiple blocks of (A/T)₄ each separated by four contiguous G•C pairs. All 16 possible combinations of (A/T)₄ sites were represented. Typical footprinting gels obtained with these two fragments are presented in Figure 3. We observed that 2,7CN-H can bind well to all (A/T)₄ blocks. However, the extent of DNase I protection varies from one block to another. For example, the footprint is more pronounced at 5'-AATT and 5'-ATTT compared to 5'-ATTA or 5'-AAAT but the difference is not large. It is clear that the 2,7 disubstituted carbazole derivative can engage in contact with each type of (A/T)₄ site.

(II) What Is the Carbazole Binding Mode in Different DNA Sequences? What Are the Primary and Secondary Binding Modes? (a) UV–Vis Absorption Spectral Changes. Addition

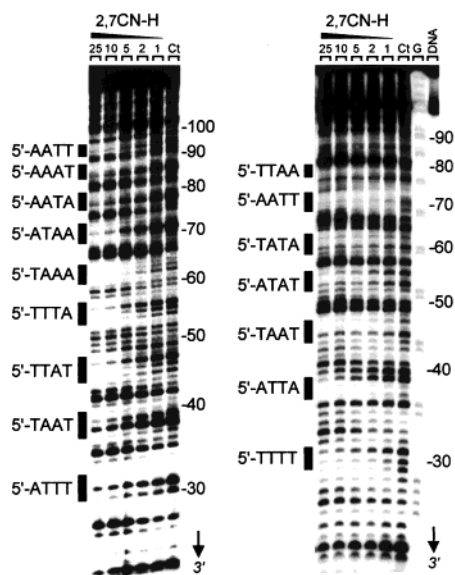


FIGURE 3: DNase I footprinting of the 2,7 substituted carbazole derivative on the restriction fragments TAYB (131 bp) and TAYD (116 bp) containing multiple blocks of (A/T)₄ each separated by four contiguous G·C pairs. (A) Fragment TAYB contains 9 blocks: AAAT, ATTA, ATAA, TAAA, TTTA, TTAT, TATT, ATTT, and AATT. (B) Fragment TAYD contains seven blocks: AAAA, TAAT, ATTA, ATAT, TATA, AATT, and TTAA. Other details are as for Figure 1.

of poly[d(A-T)]₂ to all of the carbazoles of Table 1 results in shifts of the spectra to longer wavelength and a 10–30%

decrease in extinction coefficient at the peak wavelength (Figure 4). Clearly there are strong interactions of the carbazole aromatic systems with AT base pairs for all compounds, but the interactions are sufficiently varied to induce quite different perturbations in the carbazole system. The spectral peak for the 2,6 compound (2,6CN-H) is shifted to below 300 nm and overlaps with DNA (Figures 4C) in the complex. This limits the possibilities for spectrophotometric analysis of binding with this compound.

The NMe derivatives of the 3,6 and 2,7 carbazoles have spectra in the absence of DNA that are very similar to the spectra for the corresponding NH compounds (Figure 4). The shifts induced by the AT polymer are quite similar for the 3,6 NMe and NH derivatives, suggesting that the complexes are not strongly affected by the NMe group (Figure 4A). With the 2,7 compounds, the spectral shifts are larger for the NH than for the NMe compound with the AT polymer (Figure 4B). In agreement with our proposed models (22) and Figure 11, this result suggests that the methyl group inhibits minor groove binding of the 2,7 carbazole but does not interfere with binding of the 3,6 derivatives.

(b) *Fluorescence Spectral Changes.* Fluorescence spectra of all carbazoles show large changes when titrated with poly[d(A-T)]₂ (Figure 5). Free 3,6CN-H has a strong fluorescence emission band centered at 420 nm. Addition of poly[d(A-T)]₂ causes a significant shift of the peak maximum to lower wavelength with an approximately 12% decrease in the fluorescence at the original peak wavelength

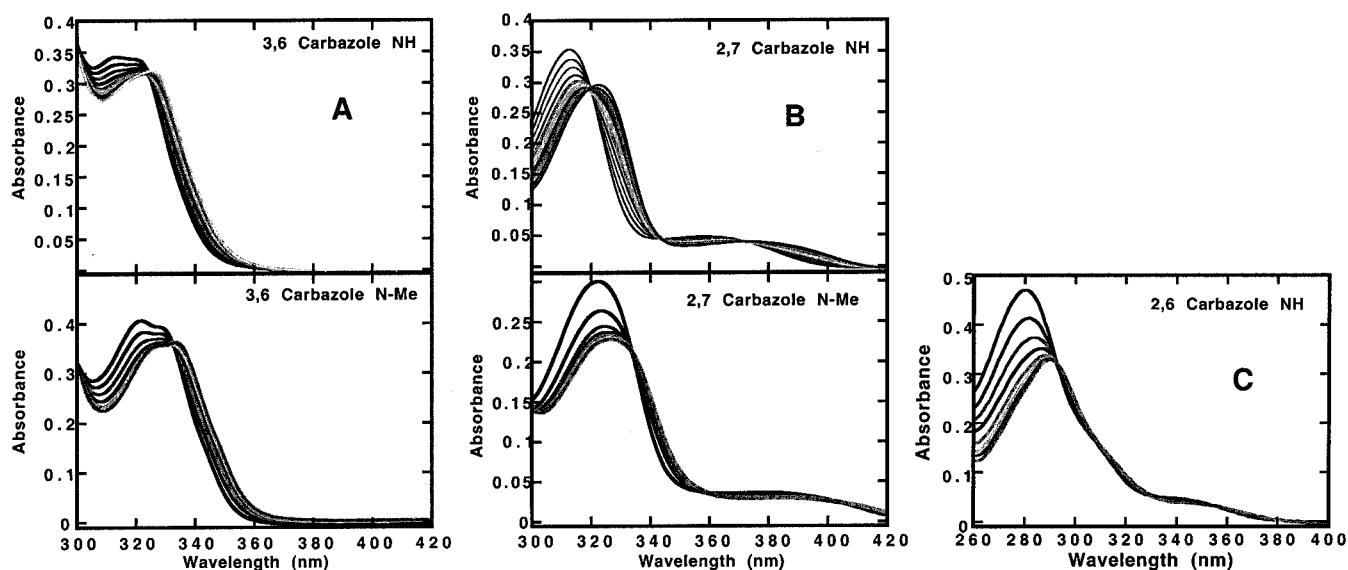


FIGURE 4: Carbazole spectrophotometric titrations. (A) Titrations of the 3,6 carbazole NH (top), and 3,6 carbazole NMe (bottom) with poly[d(A-T)]₂. Titrations were conducted in a 1 cm cell in MES buffer with 0.1 M NaCl added at 25 °C. The concentrations in the top figure are as follows: 3.121×10^{-5} M 3,6 carbazole NH, and poly[d(A-T)]₂ concentrations in base pairs of zero, 1.189×10^{-5} , 2.37×10^{-5} , 3.55×10^{-5} , 4.71×10^{-5} , 5.87×10^{-5} , 7.03×10^{-5} , 8.17×10^{-5} , 9.31×10^{-5} , 10.45×10^{-5} , and 11.57×10^{-5} , respectively from the top to the bottom curves at 312 nm. The concentrations in the bottom figure are as follows: 2.88×10^{-5} M of 3,6 carbazole NMe, and poly[d(A-T)]₂ concentrations in base pairs of zero, 1.92×10^{-5} , 3.84×10^{-5} , 5.76×10^{-5} , 7.68×10^{-5} , 9.42×10^{-5} , 11.25×10^{-5} , 13.06×10^{-5} , and 14.86×10^{-5} , respectively from the top to the bottom curves at 322 nm. (B) Titrations of the 2,7 carbazole NH (top), and 2,7 carbazole NMe (bottom) with poly[d(A-T)]₂. Titrations were conducted in a 1 cm cell in MES buffer with 0.1 M NaCl added at 25 °C. The concentrations in the top figure are as follows: 1.07×10^{-5} M 2,7 carbazole NH and poly[d(A-T)]₂ concentrations in base pairs of zero, 4.76×10^{-6} , 9.53×10^{-6} , 1.43×10^{-5} , 1.90×10^{-5} , 2.37×10^{-5} , 2.84×10^{-5} , 3.31×10^{-5} , 3.80×10^{-5} , 4.25×10^{-5} , and 4.71×10^{-5} , respectively, from the top to the bottom curves at 322 nm. The concentrations in the bottom figure are as follows: 1.0×10^{-5} M 2,7 carbazole NMe and poly[d(A-T)]₂ concentrations in base pairs of zero, 1.33×10^{-5} , 2.66×10^{-5} , 3.97×10^{-5} , 5.28×10^{-5} , 6.59×10^{-5} , 7.88×10^{-5} , and 9.17×10^{-5} , respectively, from the top to the bottom curves at 322 nm. (C) Titrations of the 2,6 carbazole NH with poly[d(A-T)]₂. Titrations were conducted in a 1 cm cell in MES buffer with 0.1 M NaCl added at 25 °C. The concentrations are as follows: 1.0×10^{-5} M 2,6 carbazole NH and poly[d(A-T)]₂ concentrations in base pairs of zero, 1.33×10^{-5} , 2.66×10^{-5} , 3.97×10^{-5} , 5.28×10^{-5} , 6.59×10^{-5} , 7.88×10^{-5} , and 9.17×10^{-5} , respectively, from the top to the bottom curves at 280 nm.

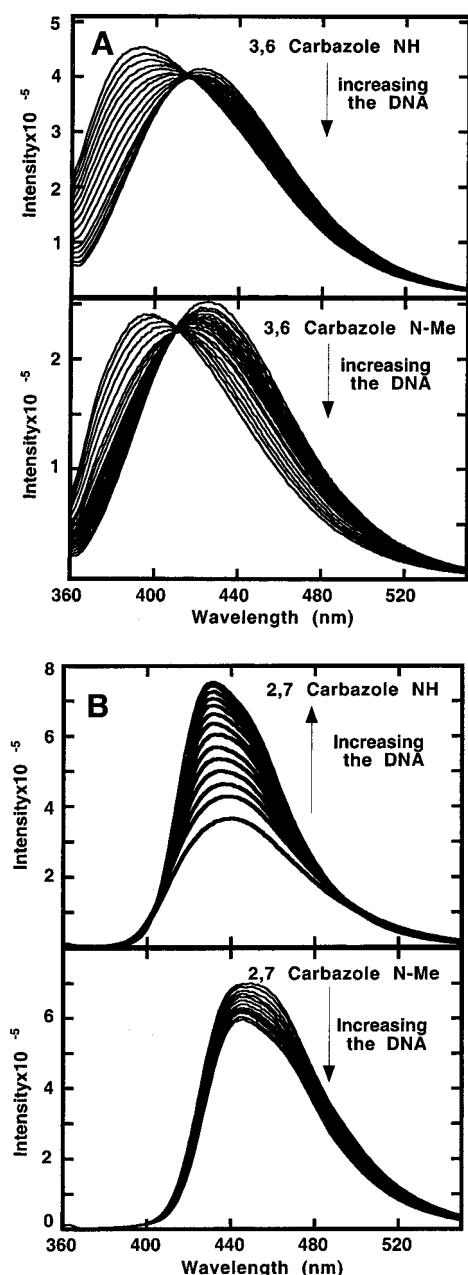


FIGURE 5: Fluorescence emission spectral titrations of the 3,6 carbazole NH and 3,6 carbazole NMe (A), and the 2,7 carbazole NH and 2,7 carbazole NMe (B) with poly[d(A–T)]₂. Titrations were conducted in a 1 cm cell with a concentration of 1×10^{-6} M of the compound in MES buffer with 0.1 M NaCl added at 25 °C. The excitation wavelength for all compounds was 320 nm, the excitation slit was at 1 nm and the emission slit at 4 nm.

(Figure 5A). Unbound 2,7CN-H has a strong fluorescence emission peak at 440 nm, and addition of poly[d(A–T)]₂ causes an approximately 100% increase in the fluorescence and a very slight shift of the peak maximum to lower wavelength (Figure 5B). Unbound 2,7CN-Me has strong fluorescence emission at 450 nm, and addition of poly[d(A–T)]₂ causes an approximately 14% decrease in the fluorescence and a very slight shift of the peak maximum to lower wavelength (Figure 5B). As with the absorption spectral results, changes caused by the AT polymer are similar for the 3,6CN-H and 3,6CN-Me derivatives, but are different with the 2,7CN-H and 2,7CN-Me derivatives (Figure 5). Addition of DNA to 2,7CN-Me, for example, results in a

quenching of fluorescence in contrast to the enhancement observed with 2,7CN-H.

(c) *Circular Dichroism (CD)*. Addition of the 3,6 carbazole (3,6CN-H) to poly[d(A–T)]₂ results in a CD decrease in the DNA region at 260 nm, and a small increase at 230 nm. There are strong positive induced CD signals at 290 and 330 nm with clear isoelliptic points at 275, 255, and 230 nm (Figure 6A). As with absorption and fluorescence results, CD changes on addition of the AT DNA are similar for the 3,6CN-H and 3,6CN-Me complexes (Figure 6A). The 2,6 derivative absorbs below 300 nm, but clear and strong induced CD bands on addition of this compound to the AT polymer are clearly visible (Figure 6C). The induced CD peaks for the carbazoles provide strong evidence of a minor groove binding mode in A/T sequences (22).

Addition of 2,7CN-H to poly[d(A–T)]₂ results in an increase of the signal at 260 nm, and small increase at 230 nm. A strong positive CD signal at 330 nm is induced with clear isoelliptic points at 230, 260, 270, and 285 nm (Figure 6B). Results with the 2,7CN-Me derivative are again different from those with the 2,7CN-H derivative on addition of the AT polymer (Figure 6B). The 2,7CN-Me compound gives very weak induced CD bands in the carbazole absorption region with the AT polymer while the induced signals for the 2,7CN-H compound are quite strong (Figure 6B).

NMR. We have previously obtained NMR results and model structures for the 2,7CN-H and 3,6CN-H compounds bound to the self-complementary oligomer, d(GCGAATTCGC)₂ (22). To obtain structural information on the DNA complexes of the new carbazole complexes, NMR spectra of the 3,6CN-Me, 2,7CN-Me, and 2,6CN-H compounds complexed with d(GCGAATTCGC)₂ were obtained. Proton chemical shifts for the compounds were assigned through a combination of 1D titration spectra, as well as 2D NOESY and COSY experiments. DNA shifts are as previously reported (22). In general, in 1D proton NMR spectra, most DNA signals are similar in line width to the free DNA but the signals for the carbazoles are exchange-broadened and below 25 °C they are difficult to observe (Figure 7). The signals become sharper as the complex moves to fast exchange at higher temperature (Figure 7). NOESY spectra in the aromatic to H1'/H5 spectral region along with a NOESY walk for assignment of the H8/H6–H1' protons are shown for the 2,6CN-H derivative in Figure 8. The H1' resonances shift very little except for the T6 and T7 signals which move substantially upfield. A cross-peak between the carbazole H1 proton signal (proton numbering of the carbazoles is in Table 1), and the H1' of T6 is seen in the NOESY plot in Figure 8. An additional cross-peak is seen between the carbazole H1 proton and A5H2 in the aromatic region of the NOESY spectrum (Supporting Information). These observations confirm a minor-groove binding mode in the central AT region of this duplex and define the 2,6CN-H orientation in the complex. As with the 2,7CN-H complex described previously (22), the 2,6CN-H binds with the carbazole NH pointed into the DNA minor groove in agreement with predictions from our models.

The complex of the 3,6CN-Me also shows downfield shifts with substantial line broadening on complex formation with d(GCGAATTCGC)₂ at low temperature (not shown). A NOESY spectrum of the aromatic to H1'/H5 spectral region provides assignment for nonexchangeable proton signals and,

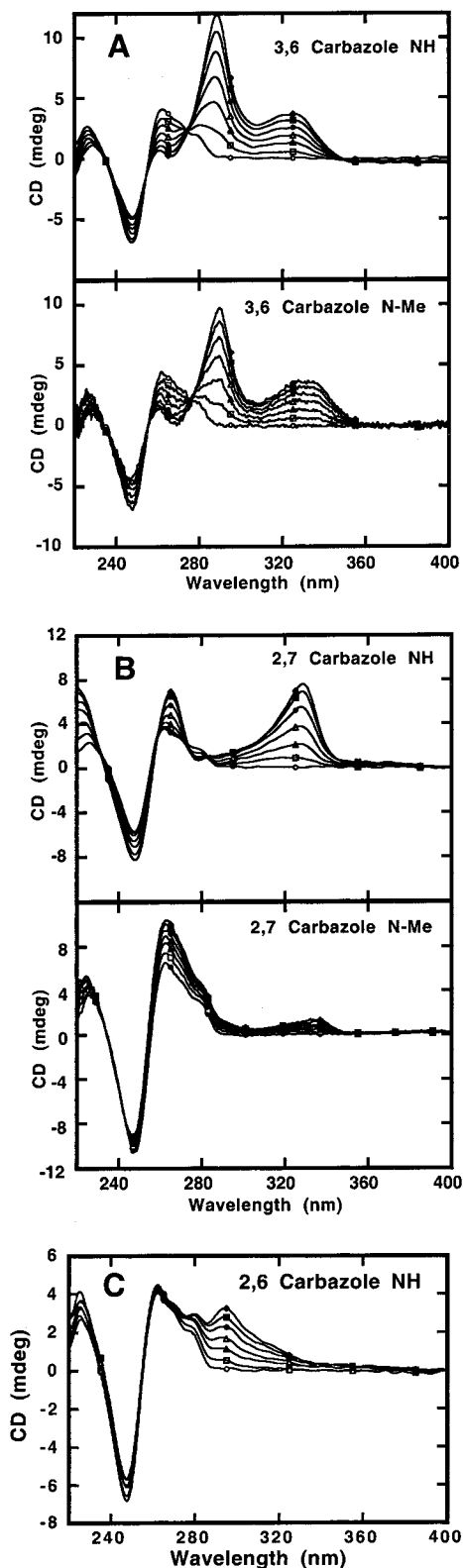


FIGURE 6: CD spectra of the carbazole compounds with poly-[d(A-T)]₂, (A) the 3,6 carbazole NH (top), and 3,6 carbazole NMe (bottom), (B) the 2,7 carbazole NH (top), and 2,7 carbazole NMe (bottom), and (C) the 2,6 carbazole NH. Experiments were conducted in a 1 cm cell in MES buffer with 0.1 M NaCl added at 25 °C. The ratio of compound/poly[d(A-T)]₂ in base pairs is 0 (○), 0.05 (□), 0.10 (▲), 0.15 (△), 0.20 (●), 0.25 (■), and 0.3 (◆).

as with the 3,6CN-H derivative, has an intermolecular cross-peak between the carbazole H4/5 and the T6H1' signals. Because of the symmetry of the 3,6 compound, in contrast

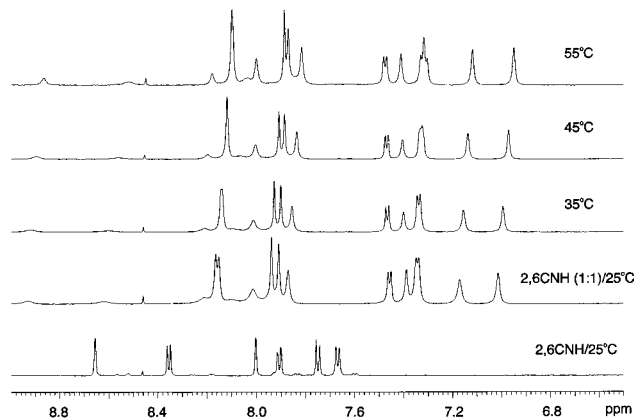


FIGURE 7: 1D proton NMR spectra of the aromatic region of the 2,6 carbazole NH complex with d(GCGAATTCGC)₂ at different temperatures are shown.

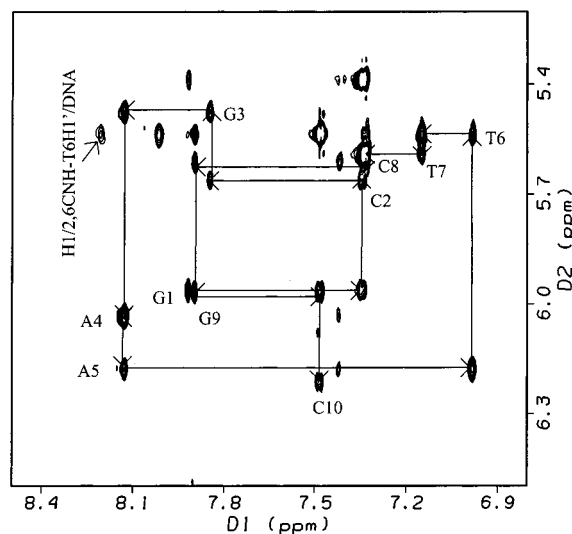


FIGURE 8: NOESY spectra in the aromatic to H1' spectral region along with a NOESY walk for assignment of H8/H6-H1' protons are shown for the 2,6 carbazole NH with d(GCGAATTCGC)₂. The experiments were conducted at 45 °C with mixing time of 300 ms.

to the 2,6 carbazole, the H4 and H5 proton signals are not distinguishable. A cross-peak is seen in the aromatic region between the carbazole H4/5 signal and A5H2 as with the 3,6CN-H derivative (22). As with the 2,6 carbazole, the T6 and T7 H1' signals show large upfield shifts on complex formation. In agreement with predictions from our models of a similar binding mode for the 3,6CN-H and 3,6CN-Me carbazoles, all NMR results with the 3,6CN-Me carbazole-oligomer complex are very similar to those previously obtained with the 3,6 NH complex (22).

The 2,7CN-Me carbazole NMR signals also broaden in complex with d(GCGAATTCGC)₂ and the chemical shift changes on complex formation similar to those for the other carbazoles. In contrast to the results obtained with the other carbazoles, no intermolecular cross-peaks are observed between the 2,7CN-Me and the DNA duplex. As with the other complexes, however, the T6 and T7 H1' signals shift significantly upfield in the 2,7CN-Me complex (Figure 9A). Base H8/H6 proton chemical shift changes are also similar for all of the carbazole complexes (Figure 9B). These results suggest that the 2,7CN-Me compound forms a minor-groove complex that is structurally similar to 2,7CN-H carbazole,

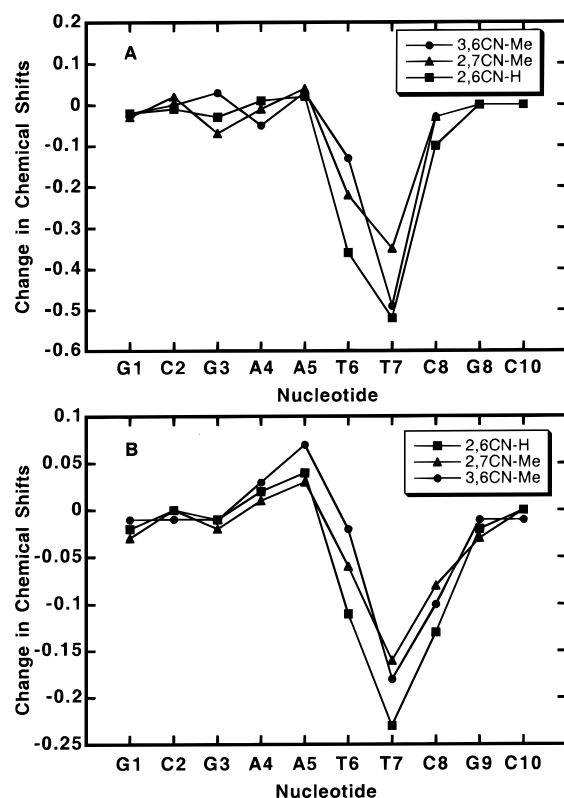


FIGURE 9: Changes in selected proton chemical shifts (complex-free) for carbazole binding to d(GCGAATTCGCG)₂ are shown. (A) H1' for the complex with 2,6 carbazole (■); 2,7 carbazole NMe (▲) and 3,6 carbazole NMe (●) (B) H8, H6 for the complex with 2,6 carbazole (■); 2,7 carbazole NMe (▲) and 3,6 carbazole NMe (●).

but with greater distances between carbazole and DNA protons. This observation strongly supports predictions from our models that the carbazole nitrogen of the 2,7 derivatives points into the DNA groove and that the complex should be severely distorted and weakened by an NMe group.

(III) *How Strongly Do the Compounds Bind to the Sequences?* To evaluate the relative affinities of the carbazoles for AT DNA sequences, T_m studies were done at a 1:1 ratio of the carbazoles to d(CGCGAATTCGCG) (Table 1). NMR results presented above show that the carbazoles are primarily bound in the minor groove at the AATT sequence in this oligomer duplex under these conditions. As expected from our models, the 3,6 amidine and imidazoline derivatives as well as the NH and NMe derivatives have similar ΔT_m values (Table 1). The amidine and imidazoline derivatives also have similar ΔT_m values for the 2,7 CH derivative and the ΔT_m values are greater than for the corresponding 3,6 derivatives. The NMe substituted 2,7 carbazole has a T_m that is significantly lower than the ΔT_m for the NH compound, again as predicted. Unexpectedly, the 2,6 carbazole has a ΔT_m that is substantially lower than that for the 2,7 compound even though NMR results show that they bind to DNA in the same orientation.

In contrast to T_m measurements, SPR binding experiments are conducted at constant temperature and they provide a more quantitative comparison of the DNA interactions of the carbazole compounds. A set of sensorgrams (response units, RU, versus time) at different carbazole concentrations for the 2,7CN-H compound binding to the AATT oligomer

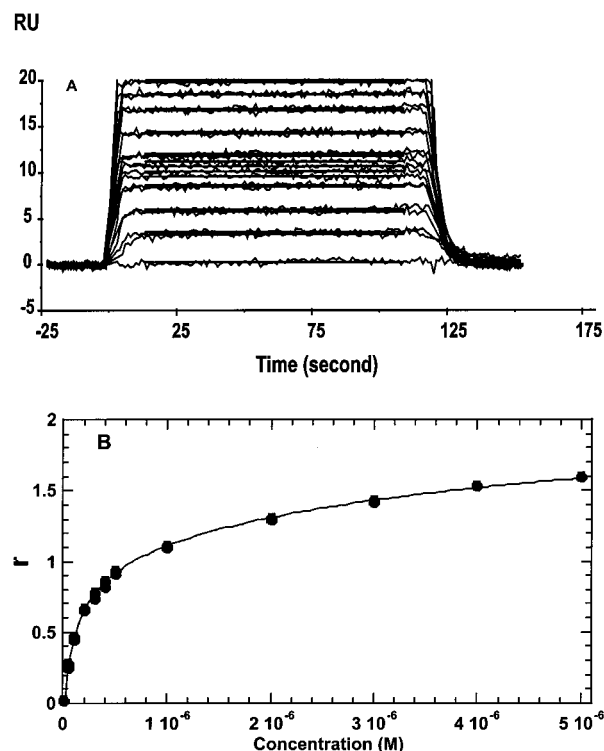


FIGURE 10: Carbazole-DNA equilibrium constants. (A) A set of SPR sensorgrams for binding of 2,7 carbazole NH to the AATT sequence hairpin in MES buffer with 0.1 M NaCl at 25 °C are shown. The unbound carbazole concentrations in the flow solution range from 50 nM in the lowest curve to 5 μM in the top curve. The lines in the figure are linear best fits to the steady-state RU values and were used to determine the RU for each free ligand concentration. (B) Determination of the affinity constant for the 2,7 carbazole NH–AATT hairpin complex from the data in Figure 10A. The r values determined by using eqs 1 and 2 and RU values from the steady-state region from the figure are plotted versus the unbound carbazole concentration. The results were fit by nonlinear least-squares methods to a two-site model (eq 3).

hairpin are shown in Figure 10A as examples of results for all of the carbazoles. As can be seen, the carbazoles bind rapidly to this DNA sequence and reach a stable steady-state plateau. Dissociation is also rapid and the DNA surface is regenerated by buffer flow without additional regeneration reagents.

The instrument response (RU) in the steady-state region is proportional to the amount of bound carbazole and was determined by linear-averaging over a 90 s time span (Figure 10A).

The predicted maximum response per bound compound in the steady-state region (RU_{max}) can be calculated by eq 1:

$$RU_{\max} = RU_{\text{AATT hairpin immobilized}} \times \left(\frac{\text{MW compound}}{\text{MW DNA}} \right) \times RI \quad (1)$$

where the first term on the right side of eq 1 is for the RUs of nucleic acid that were immobilized, the second term is the ratio of molecular weights of the compound and nucleic acid, and the third term is the refractive index gradient ratio for the compound and DNA. We have found by using differential refractometry that the RI values of a number of minor-groove cations with extended conjugation, such as the carbazoles of Table 1, are approximately 1.4 under our conditions (34). The RU_{max} value is required to convert the

Table 3: SPR Analysis of Carbazole Dication Binding to the DNA Hairpin Oligomer with Stem Sequence CGAATTCG^a

compd	K_1 (M ⁻¹)	K_2 (M ⁻¹)
2,7CN-H	6.1×10^6	3.0×10^5
2,7CN-Me	1.2×10^6	2.5×10^5
3,6CN-H	3.5×10^6	4.2×10^5
3,6CN-Me	4.6×10^6	3.5×10^5
2,6CN-H	2.7×10^6	3.5×10^5

^a Equilibrium constants for carbazole–DNA complexes were determined at 25 °C in MES10 buffer.

observed response (RU) to the standard binding parameter, r (moles of compound bound/mole of AATT hairpin):

$$r = \text{RU}/\text{RU}_{\text{max}} \quad (2)$$

Steady-state RU values (such as in Figure 10A) were converted to r according to eq 2, and the results for binding of the 2,7CN-H to the DNA hairpin duplex at 25 °C are plotted in Figure 10B. The results were fit by nonlinear least-squares methods to a two-site equilibrium model, eq 3, and results for all compounds determined in this manner are collected in Table 3:

$$r = (K_1 C_{\text{free}} + 2K_1 K_2 C_{\text{free}}^2) / (1 + K_1 C_{\text{free}} + K_1 K_2 C_{\text{free}}^2) \quad (3)$$

where C_{free} is the unbound compound concentration in equilibrium with the DNA–compound complex and is fixed by the compound concentration in the flow solution. K_1 and K_2 values are the macroscopic equilibrium constants for binding to the two sites and are given in Table 3. Since in all cases the observed RU values at high compound concentrations were greater than RU_{max} , the compounds must have at least two binding sites on this DNA sequence. This is in agreement with our previous observations that carbazoles can bind by intercalation at GC sites with binding constants that are significantly lower than for the primary minor groove complex (22). The K_1 values are 10–20-fold greater than for K_2 and represent the equilibrium constant for binding to the DNA minor groove in the AATT sequence of the oligomer.

In excellent agreement with T_m determinations (Table 1) and with affinity conclusions from foot printing experiments (Figures 1–3), the 2,7CN-H compound has a higher binding constant than the 3,6CN-H and 2,6CN-H derivatives. The 2,7CN-Me derivative has the lowest K_1 value. The 3,6CN-H and 3,6CN-Me derivatives have similar binding constants in agreement with predictions from our binding models. As predicted by the T_m experiments, the 2,6 carbazole binds more weakly than either the 2,7CN-H or the 3,6CN-H derivatives.

DISCUSSION

In previous studies with 2,7 and 3,6 substituted carbazole imidazoline derivatives, we presented evidence that despite their structural differences, both compounds bind strongly in the minor groove at AT DNA sequences (22). NMR and molecular modeling studies produced a surprising model in which the 2,7 carbazole binds in AT sequences with hydrogen bonds involving one imidazoline group and the carbazole NH. The 3,6 compound, however, is predicted to

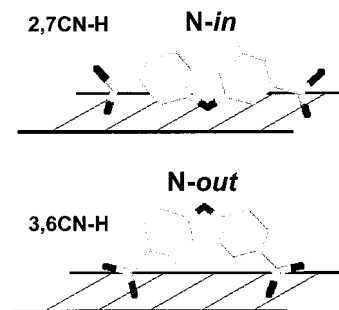


FIGURE 11: Schematic illustrations to show the orientation of the 2,7CN-H and 3,6CN-H carbazoles with respect to the DNA minor groove surface.

bind in a more “classical” model that uses both imidazoline groups for H-bonding with the carbazole NH pointed out of the minor groove. The models thus predict that both 2,7 and 3,6 carbazoles form minor groove complexes with AT sequences but that the complexes have quite different structures with the carbazoles oriented in the groove in an opposite manner (22), as diagramed in Figure 11.

Given that these proposed models differ considerably from the classical minor-groove paradigm for unfused aromatic dications, for example, X-ray results with other dications (10), we have now tested them with new derivatives and experimental methods. As noted in the introductory portion of this paper, amidine compounds are predicted by the models to bind similarly to imidazolines. The NMe derivatives are predicted to bind similarly to the CN-H compound with the 3,6 substitution, but much weaker than the CN-H compound with the 2,7 substitution. The 2,6 compound is predicted to form a complex that is similar to the 2,7 complex. Spectroscopic analysis presented in Figures 4–6 strongly supports these predictions. The 3,6 NH and NMe derivatives have similar spectroscopic characteristics that indicate minor groove binding in AT sequences with the carbazole N pointed out. In agreement with the predicted 2,7 model with the carbazole N pointed into the groove, the NMe derivative has quite different spectroscopic properties than the NH compound.

Spectroscopic determination of binding constants of the carbazoles with DNA is difficult for several reasons: (i) the compounds have secondary binding (probably intercalation) that is generally about a factor of 10 weaker than the minor groove binding for some compounds; (ii) the compounds do not have very strong spectroscopic signals; (iii) at low concentrations absorption to spectrophotometer cells can affect the solution concentration of the compounds; (iv) with the 2,6 carbazole the spectrum overlaps the DNA spectrum. We have found, however, as with other minor groove binding agents (35) that we can obtain reproducible and accurate equilibrium constants under a variety of conditions with SPR-biosensor methods. SPR determines the bound ligand concentration, and fixes the unbound ligand concentration in the flow solution. Where spectroscopic results are available, the agreement with SPR equilibrium constants is excellent (35). The SPR binding constants for minor groove interactions are in the order $2,7\text{CN-H} > 3,6\text{CN-Me} > 3,6\text{CN-H} > 2,6\text{CN-H} > 2,7\text{CN-Me}$. Footprinting results with the NH carbazoles are in complete agreement with these findings. The 2,7 carbazole produces much stronger footprints than either the 3,6 or the 2,6 derivatives. All of these results again

support the models that predict that the 3,6 complex is different than the 2,7 carbazole complex.

All three types of carbazole derivatives produce footprints that indicate AT binding specificity in a minor groove complex. The strongest foot prints are obtained with the 2,7CN-H derivative (Figure 1). Secondary inhibition of the enzyme at high ratios (probably through compound intercalation) is more pronounced with the 3,6 derivative than with 2,7CN-H, however, indicating that secondary binding competes more effectively with minor groove interactions with the 3,6 compounds. This is again in agreement with SPR results that show relatively stronger primary to secondary binding constants for the 2,7 carbazole relative to the other derivatives (Table 2). Interestingly, the 2,7 carbazole, in particular, can produce strong cleavage enhancements in some extended GC sequences in addition to its protection from cleavage in AT sequences. The carbazoles have a clear binding preference for AT base pair containing sites that have four or more AT base pairs, but the preference for specific AT sequences in these sites is not strong. The 2,7CN-H, for example, binds better to AATT than to ATTA and better to ATTT than to AAAT (all 5'–3') but the difference is not large.

In conclusion, these results are in excellent agreement with our previous findings and confirm that the carbazoles bind specifically in the minor groove in AT sequences. Secondary interactions, which are probably due to intercalation of the carbazoles, are 10–50-fold weaker than the minor groove interactions. New NMR results and results with new NMe derivatives strongly support our previously proposed models with the carbazole N pointed into the groove in the 2,7 complex and out of the groove in the 3,6 complex. The 2,7CN-H derivative is clearly able to better optimize all interactions with DNA such that it has a higher binding constant for AT sequences than the 3,6CN-H compound with its more classical minor groove binding shape.

SUPPORTING INFORMATION AVAILABLE

NOESY spectrum showing the cross-peak between the 2,6 carbazole H1 proton and A5H2 in the aromatic region at 45 °C with a mixing time of 300 ms (Figure 1S). This material is available free of charge via the Internet at <http://pubs.acs.org>.

REFERENCES

1. Tidwell, R. R., and Bell, C. A. (1994) in *Pneumocystis carinii pneumonia* (Walzer, P. D., Ed.) 2nd ed., revised and expanded, pp 561–583, Marcel Dekker, Inc., New York.
2. Bell, C. A., Cory, M., Fairley, T. A., Hall, J. E., and Tidwell, R. R. (1991) *Antimicrob. Agents Chemother.* 35, 1099–1107.
3. Bell, C. A., Dykstra, C. C., Aiman, N. A. I., Cory, M., Fairley, T. A., and Tidwell, R. R. (1993) *Antimicrob. Agents Chemother.* 37, 2668–2673.
4. Dykstra, C. C., and Tidwell, R. R. (1991) *J. Protozool.* 38, 78S–81S.
5. Zimmer, C., and Wahnert, U. (1986) *Prog. Biophys. Mol. Biol.* 47, 31–112.
6. Kopka, M. L., and Larsen, T. A. (1992) in *Nucleic Acid Targeted Drug Design* (Propst, C. L., and Perun, T. J., Eds.) pp 303–374, Marcel Dekker, Inc., New York.
7. Kopka, M. L., Yoon, C., Goodsell, D., Pjura, P., and Dickerson, R. E. (1985c) *Proc. Natl. Acad. Sci. U.S.A.* 82, 1376–1380.
8. Coll, M., Frederick, C. A., Wang, A. H.-J., and Rich, A. (1987) *Proc. Natl. Acad. Sci. U.S.A.* 84, 8385–8389.
9. Geierstanger, B. H., and Wemmer, D. E. (1995) *Annu. Rev. Biophys. Biomol. Struct.* 24, 463–493.
10. Neidle, S. (1997) *Biopolymers* 44, 105–121.
11. Bailly, C. (1998) in *Advances in DNA Sequence Specific Agents* (Palumbo, M., Ed.) Vol. 3, pp 97–156, JAI Press, Inc.
12. Bailly, C., and Chaires, J. B. (1998) *Bioconjugate Chem.* 9, 513–538.
13. Wilson, W. D. (1996) in *Nucleic Acids in Chemistry and Biology* (Blackburn, G. M., and Gait, M. J., Eds.) 2nd ed., Chapter 8, IRL Press.
14. Wilson, W. D., Tanious, F. A., Barton, H. J., Jones, R. L., Fox, K., Wydra, R. L., and Strekowski, L. (1990) *Biochemistry* 29, 8452–8461.
15. Wilson, W. D., Tanious, F. A., Buczak, H., Ratmeyer, L., Venkatramanan, M. K., Kumar, A., Boykin, D. W., and Munson, R. (1992) in *Structure and Function, Vol. 1: Nucleic Acid* (Sarma, R. H., and Sarma, M. H., Eds.) pp 83–105, Adenine Press, Schenectady, NY.
16. Edwards, K. J., Jenkins, T. C., and Neidle, S. (1992) *Biochemistry* 31, 7104–7109.
17. Fairley, T. A., Tidwell, R. R., Donkor, I., Naiman, N. A., Ohemeng, K. A., Lombardy, R. J., Bentley, J. A., and Cory, M. (1993) *J. Med. Chem.* 36, 1746–1753.
18. Boykin, D. W., Kumar, A., Sychala, J., Zhou, M., Lombardy, R. J., Wilson, W. D., Dykstra, C. C., Jones, S. K., Hall, J. E., Tidwell, R. R., Laughton, C., Nunn, C. M., and Neidle, S. (1995) *J. Med. Chem.* 38, 912–916.
19. Tidwell, R. R., Geratz, J. D., Dann, O., Volz, G., and Zeh, D. (1978) *J. Med. Chem.* 21, 613–623.
20. Tidwell, R. R., Jones, S. K., Naiman, N. A., Berger, I. C., Brake, W. R., Dykstra, C. C., and Hall, J. E. (1993) *Antimicrob. Agents Chemother.* 37, 1713–1716.
21. Patrick, D. A., Boykin, D. W., Wilson, W. D., Tanious, F. A., Sychala, J., Bender, B. C., Hall, J. E., Dykstra, C. C., Ohemeng, K. A., and Tidwell, R. R. (1997) *Eur. J. Med. Chem.* 32, 781–793.
22. Tanious, F. A., Ding, D., Patrick, D. A., Tidwell, R. R., and Wilson, W. D. (1997) *Biochemistry* 36, 15315–15325.
23. Wilson, W. D., Wang, Y.-H., Kusuma, S., Chandrasekaran, S., Yang, N. C., and Boykin, D. W. (1985) *J. Am. Chem. Soc.* 107, 4989–4995.
24. Fasman, G. D. (1975) in *Nucleic Acids* (Fasman, G. D., Ed.) pp 589, CRC Press, Cleveland, OH.
25. Kerckaert, J. P., Dewindt, C., Tilly, H., Quief, S., Lecocq, G., Bastard, C. (1993) *Nat. Genet.* 5, 66–70.
26. Lamond, A. I., and Travers, A. A. (1983) *Nature* 305, 248–250.
27. Bailly, C., and Waring, M. J. (1995) *J. Biomol. Struct. Dyn.* 12, 869–898.
28. Wilson, W. D., and Lopp, I. G. (1979) *Biopolymers* 18, 3025–3041.
29. Wilson, W. D., Krishnamoorthy, C. R., Wang, Y.-H., and Smith, J. C. (1985) *Biopolymers* 24, 1941–1961.
30. Kibler-Herzog, L., Kell, B., Zon, G., Shinozuka, K., Mizan, S., and Wilson, W. D. (1990) *Nucleic Acids Res.* 18, 3545–3555.
31. Wilson, W. D., Tanious, F., Barton, H., Jones, R., Strekowski, L., and Boykin, D. (1989) *J. Am. Chem. Soc.* 111, 5008–5010.
32. States, D. J., Haberkorn, R. A., and Ruben, D. J. (1982) *J. Magn. Reson.* 48, 286–292.
33. Goodisman, J., and Dabrowiak, J. C. (1992) *Biochemistry* 31, 1058–1064.
34. Davis, T. A., and Wilson, W. D. (2000) *Anal. Biochemistry* (in press).
35. Mazur, S., Tanious, F. A., Ding, D., Kumar, A., Boykin, D. W., Simpson, I. J., Neidle, S., and Wilson, W. D. (2000) *J. Mol. Biol.* 300, 321–337.